ACS OMEGA

Article

Cite This: ACS Omega 2019, 4, 1897−1906

http://pubs.acs.org/journal/acsodf

Facile Preparation of Hierarchical AgNP-Loaded MXene/Fe_3O_4/Polymer Nanocomposites by Electrospinning with Enhanced Catalytic Performance for Wastewater Treatment

Xinxin Huang,[†,‡,§] Ran Wang,[‡,§] Tifeng Jiao,*[,†,‡] Guodong Zou,[‡] Fangke Zhan,[‡] Juanjuan Yin,[‡] Lexin Zhang,[‡] Jingxin Zhou,[‡] and Qiuming Peng*[,†]

[†]State Key Laboratory of Metastable Materials Science and Technology and [‡]Hebei Key Laboratory of Applied Chemistry, School of Environmental and Chemical Engineering, Yanshan University, Qinhuangdao 066004, China

ABSTRACT: MXene as a kind of two-dimensional nanomaterial has aroused people's strong research interest because of its excellent properties. In the present study, we introduced a new poly(vinyl alcohol)/poly(acrylic acid)/Fe_3O_4/MXene@Ag nanoparticle composite film fabricated by electrospinning and heat treatment as well as self-reduction reaction process. The obtained composite films showed high self-reduction ability because of the incorporation of MXene flakes. The intercalated MXene flakes in the composite nanofibers were evenly distributed, which not only solved the aggregation problem from MXene dispersion but also could self-reduce Ag nanoparticles in situ in composite materials. In addition, the composite nanofiber films exhibited good fiber structure, thermal stability, and magnetic properties. Moreover, the composite nanofiber films demonstrated excellent catalytic ability and cycle stability to 4-nitrophenol and 2-nitroaniline.

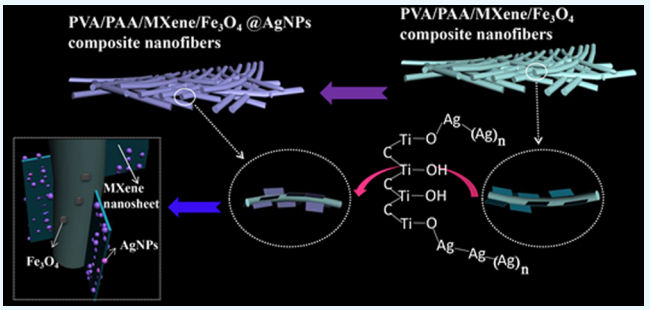

1. INTRODUCTION

In recent years, MXene's extraordinary physical and chemical properties and layered structure have made it a new type of two-dimensional (2D) material that is popular after graphene.[1−3] MXene is a transition metal nitride/carbon nano-2D layered material that was first prepared by Naguib in 2011.[4] The structure of MXene can be represented by $M_{n+1}X_nT_x$.[5] In short, M represents a transition metal element, X represents a C or N element, and T_x represents a functional terminal such as −O, −OH, −F, and so on.[6] In this structural formula, n can take 1, 2, or 3.[7] MXene is a layered material obtained by etching away the Al layer by MAX.[8] It has great application prospects in electrochemistry, magnetism, and optic fields.[9−20] Particularly, the MXene flake obtained by delaminating is one of the most valuable nanomaterials.[21−25] The nanosheet has a large specific surface area and can be used in the production of new functional hybrid material building blocks.[26−30] However, the MXene nanosheets are easy to aggregate in solution and oxidized easily, which have become a challenge that needs to be solved urgently.

To solve these problems, the researchers focused on the separation of flakes and the modification of the surface MXene flakes. For example, Wang et al. stratified MXene by modification of sulfonic acid diazonium salts and ultrasound.[9] The obtained large-scale MXene flakes have stable properties and not easy to agglomerate. Boota et al. prepared PPy/$Ti_3C_2T_x$ composites by modifying polypyrrole on the surface of MXene sheets.[7] It was found that pyrrole (C_4H_4NH) can simultaneously be embedded, aligned, and metal-free polymerized on $Ti_3C_2T_x$ MXene. In addition, PPy/$Ti_3C_2T_x$ composite exhibits excellent electrochemical properties. Ling et al. prepared $Ti_3C_2T_x$/polymer flexible composite material by mixing MXene ($Ti_3C_2T_x$) with charged polydiallyldimethylammonium chloride or electrically neutral polyvinyl alcohol (PVA), which can enhance cation embedding and increase capacitance, and has a high potential for electrochemical applications.[11] Researchers have indeed made outstanding contributions in fully exploiting MXene. However, the problem of easy aggregation of MXene sheets has not been completely solved. In addition, its self-reducing precious metal properties are masked after the MXene flakes' surface has been modified. On the other hand, self-assembled composites are widely prepared and applied because of their good properties.[31−33] Nitro compounds are one of the common water pollutants. In particular, 4-nitrophenol (4-NP) and 2-nitroaniline (2-NA) are typically harmful compounds for humans and environment because of their high solubility and toxicity. Therefore, it is very important to develop new materials that can effectively catalyze 4-NP and 2-NA.[34,35]

To solve the problems mentioned above, we designed and successfully synthesized PVA/poly(acrylic acid)/Fe_3O_4/MXene@AgNP (PVA/PAA/Fe_3O_4/MXene@AgNP) functional nanocomposites in combination with the electrospinning technology. It is well-known that the electrospinning

Received: December 23, 2018
Accepted: January 10, 2019
Published: January 24, 2019

DOI: 10.1021/acsomega.8b03615
ACS Omega 2019, 4, 1897−1906

technology is a technology capable of producing continuous microfilaments with a diameter scale of nanometer or micrometer. The morphology, diameter scale, and stacked density of fibers can be regulated by adjusting process parameters and environmental conditions.[36] In our research, the solvent used ultrapure water, and the spinning materials were PVA and PAA, all of which were water soluble and ecofriendly materials, nonpolluting, and easily degradable. Fe_3O_4 was added to the spinning material, and the composite nanofiber materials could exhibit magnetic properties.[37−40] Moreover, Fe_3O_4 was easy to recycle.[37] The MXene flake colloidal solution was obtained by dispersing MXene powder in dimethyl sulfoxide (DMSO) for later experiments.[41] The composite nanofiber materials were prepared by mixing PVA, PAA, Fe_3O_4, and MXene components via the electrospinning technology and next modification with Ag nanoparticles (AgNPs).[42] This obtained composite fiber material not only made full use of the self-reducing properties of MXene sheet itself but also solved the aggregation problem from MXene dispersion. The MXene flakes were stretched out on the surface of the obtained fiber. The reduction characteristics of the MXene nanosheet itself could reduce Ag^+ in the $AgNO_3$ solution to AgNPs at the active site on the surface of the nanosheet.[41,42] As reaction time continued, AgNPs grew and aggregated, eventually forming Ag nanoclusters.[8,41] In this report, we explored the synthesis and characterization of novel PVA/PAA/Fe_3O_4/MXene@AgNP composite nanofibers. This composite fiber material exhibited excellent properties for catalytic reduction of nitro compounds such as 2-NA and 4-NP.[43,44] In addition, we investigated the size of self-reduced AgNPs and their catalytic effects on 2-NA and 4-NP at different reduction times.[45−48] The experimental results showed that the prepared PVA/PAA/Fe_3O_4/MXene@AgNP composite nanofibers demonstrated a great potential in the field of composite catalyst materials and wastewater treatment.

2. RESULTS AND DISCUSSION

2.1. Preparation and Characterization of Composite Fibers. First, Figure 1 indicated the preparation process of PVA/PAA/Fe_3O_4/MXene@AgNP composite nanofibers. We exfoliated layered MAX (Ti_3AlC_2) powders by treating them in 40% HF solution at 25 °C.[42] Selective HF etching originated from only "A" layers from the MAX phase.[49] Then, MAX

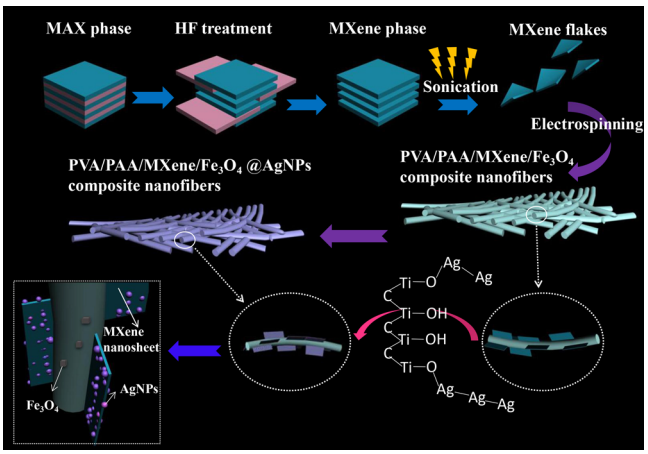

Figure 1. Schematic illustration of the preparation process of the present composite fibers.

became a multilayer MXene phase. In many cases, such as thermal treatment, sonication and reactions of volume expansion in the interlayer space would lead to deintercalation of some certain compounds and exfoliation.[50] DMSO has been reported to intercalate MXene at room temperature because DMSO could increase the c-lattice parameter of MXene from 19.5 ± 0.1 to 35.04 ± 0.02 Å.[50] The DMSO-intercalated MXene sonicated in water lead to themselves being delaminated into separate flakes similar to "paper" and formation of nanosheet colloidal solution.[41] Multilayer MXene was intercalated with DMSO and ultrasonically dispersed to obtain MXene nanosheet colloidal solution for the next step of electrospinning. PVA, PAA, Fe_3O_4, and MXene nanosheet colloidal solution were mixed in proportion to form an electrospinning precursor solution. Through electrospinning, we obtained composite nanofibers with MXene flake "wings". When the composite nanofibers were placed in a slowly stirred $AgNO_3$ solution, a [Ag^+-DMSO] complex monomer was first formed.[41] The rapidly transferred electrons form oxygen lone pair electrons ([ÖS−$(CH_3)_2$]) leading to the formation of Ag^+−[DMSO].[41] The charge was transferred between Ag−MXene complexes to initialize the dimerized MXene−Ag DMSO.[41] The MXene−Ag dimeric complexes were bonded to −OH and reduced to stable Ag^0 nanoclusters.[41,42] As the nanoclusters were further nucleated and grown on the surface of the MXene nanosheets, spherical AgNPs were formed.[41,42] With the increment of self-reduction time, they may have a small amount of AgNPs drifted/anchored on the surface of polymer fibers. Finally, the AgNP-loaded composite nanofibers were successfully prepared. It should be noted that the layered MXene nanosheets were firmly "locked" on the fiber surface by composite nanofibers to achieve high dispersibility, which solved the problem that MXene nanosheets were easy to aggregate. In addition, the MXene flakes were not modified by any functional groups, and their original properties were preserved. This experiment is based on the reaction mechanism of in situ formation of AgNP@MXene hybrids.[42] The MXene nanosheet has a large specific surface area, and the surface has a reduction/nucleation site of the original AgNPs. Furthermore, the surface of MXene contains an −OH functional group, which can bond with Ag^+ ions.[41] Over enough time, AgNPs continue to grow to form stable Ag nanospheres on the fiber surface. The composite nanofibers used to catalyze 4-NP and 2-NA also obtained good catalytic effects.

Scanning electron microscopy (SEM) image of Figure 2a showed that the MXene with layered structure by etching off the Al layer was clearly visible. A drop of the MXene nanosheet colloidal solution was deposited on a copper foil, and the nanosheets were clearly observed though SEM (Figure 2b) after being dried at 70 °C. It was clear from Figure 2 that the nanosheets were very thin and evenly distributed. Figure 2c demonstrated that the average size of the nanosheets was 350 nm. The photograph of Figure 2c′ represented a colloidal solution of MXene nanoflakes that exhibited the Tyndall scattering effect when the beam passed through. Figure 2d demonstrated clearly that the representative MXene flakes were thin and stacked.

Figure 3 showed the composite nanofibers with different micromorphology. The SEM image in Figure 3a showed PVA/PAA uniform nanofibers with the optimal parameter of 15 kV-20 cm-0.5 mL/h and the average size of the diameter of 500 nm. The SEM image (Figure 3b) of PVA/PAA/Fe_3O_4/MXene

DOI: 10.1021/acsomega.8b03615
ACS Omega 2019, 4, 1897−1906

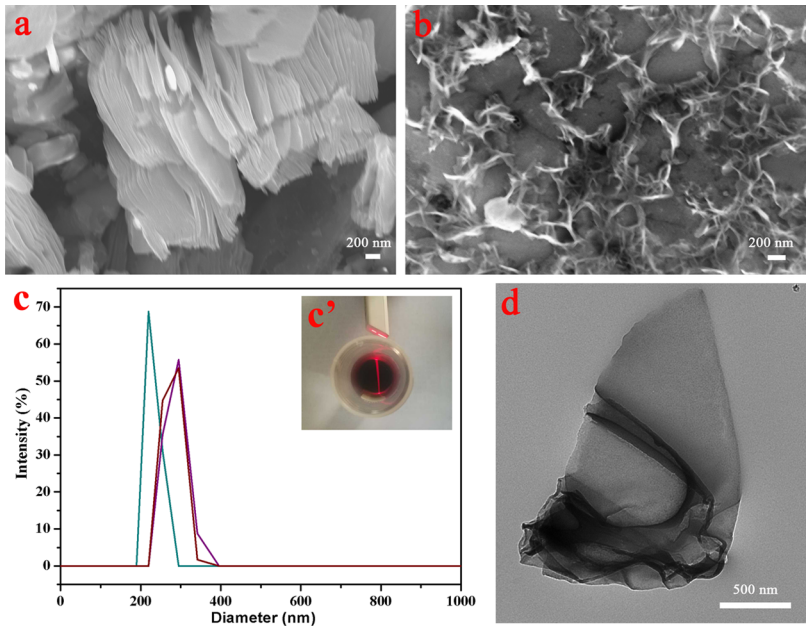

Figure 2. (a) Typical SEM image of the MXene phase after etching Al layer; (b) typical SEM image of MXene flakes; and (c) size distribution of MXene flakes. The inset image (c′) denoted MXene flakes colloidal solution with Tyndall scattering effect and (d) representative TEM image of MXene flakes.

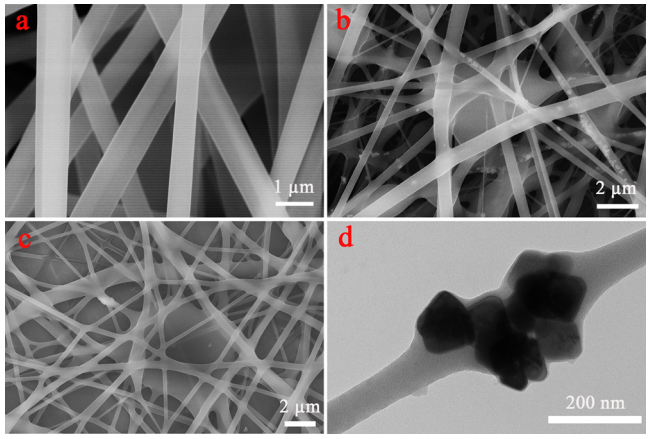

Figure 3. SEM images of (a) PVA/PAA nanofibers; (b) PVA/PAA/Fe_3O_4/MXene nanofibers; (c) PVA/PAA/Fe_3O_4/MXene nanofibers with thermal treatment for 5 h; and (d) typical TEM image of cube Fe_3O_4 NPs inside nanofiber.

composite nanofibers demonstrated that the morphology of the fibers changed after Fe_3O_4 and MXene were added under same parameters. From Figure 3b, it could be easily seen that some Fe_3O_4 particles appeared in the fiber. Furthermore, local fusion between the fibers occurred, which could be caused by the presence of a small number of micron-sized MXene large layers. The fiber diameter became uneven. Figure 3c showed that a SEM image of the PVA/PAA/Fe_3O_4/MXene composite nanofibers appeared cross-linked in plane after thermal treatment at 120 °C for 5 h. Fe_3O_4 nanocubes with an average size of 100 nm embedded in the composite nanofibers were clearly visible, as shown in Figure 3d. The presence of Fe_3O_4 NPs made the composite fibers magnetic and recyclable.

As shown in Figure 4a, it clearly showed that the surface of the fiber was embedded with the MXene nanosheets similar to the fiber growing "wings". It could be clearly seen from the partially magnified transmission electron microscopy (TEM) image (Figure 4b) of the composite nanofiber that the AgNPs were loaded onto the MXene nanosheet. This confirmed that PVA/PAA/Fe_3O_4/MXene@Ag composite nanofibers were successful prepared. Figure 4c further confirmed Fe_3O_4, MXene, and AgNP coexisted and distributed in the obtained composite nanofibers. In addition, energy-dispersive X-ray (EDX) spectroscopy shown in Figure 4d demonstrated that the elements of C, O, Fe, Ti, and Ag were presented in PVA/PAA/Fe_3O_4/MXene@AgNP composite nanofibers, indicating the successful preparation of composite nanofibers again.

High-resolution TEM (HRTEM) images demonstrated that AgNPs were single crystals. In the process of Ag reduction in situ by MXene flakes, with the increase of reduction time, AgNPs grew slowly. Figure 5b,e,h showed the interplanar spacing of lattice with $d(111)$ of 0.238 nm and $d(200)$ of 0.208 nm.[37] The formed AgNPs showed the average particle size of 12 ± 5 nm at 10 min, as shown in Figure 5c. Furthermore, AgNPs in composite nanofibers displayed an average size of 17 ± 5 nm (Figure 5f) at 20 min and 22 ± 5 nm (Figure 5i) at 60 min, respectively, which indicated the slow increment of AgNP particle size with the reduction reaction time.

X-ray diffraction (XRD) data were used to identify strong affiliation in composite nanofibers. Figure 6a indicated the diffraction patterns of the MXene powder, Fe_3O_4 NPs, PVA/PAA nanofibers, PVA/PAA/Fe_3O_4/MXene composite nanofibers, and PVA/PAA/Fe_3O_4/MXene@AgNP composite nanofibers. XRD curves of the MXene powder clearly indicated the peaks at 2θ = 8.90°, 18.24°, and 27.65° which was attributed to (002), (006), and (008) crystal plane, respectively.[42,43] According to the XRD patterns of the face-centered cubic Fe_3O_4 phase, the 2θ values were observed at 30.0°, 35.3°, 43.0°, 57.0°, and 62.7° which were attributed to the (220), (311), (400), (511), and (400) crystal planes.[37−40] The peaks of XRD were observed at 20.24° (PVA/PAA) and 19.29° (PVA/PAA/Fe_3O_4/MXene), which indicated the addition of the Fe_3O_4 NPs and MXene flakes in the composite nanofiber layers.[37] In addition, the inset shows the characteristic peaks of

DOI: 10.1021/acsomega.8b03615
ACS Omega 2019, 4, 1897−1906

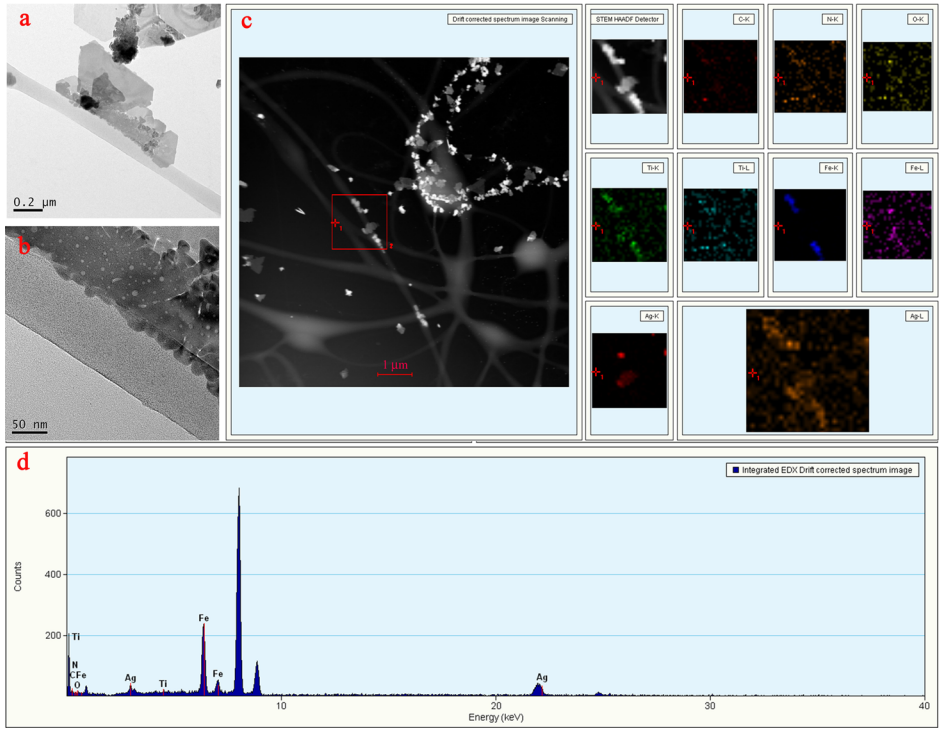

Figure 4. (a) Representative TEM image of PVA/PAA/Fe_3O_4/MXene@AgNP nanofiber; (b) partial magnification TEM image of nanofibers; (c) TEM image with C/O/Fe/Ti/Ag elemental mapping of PVA/PAA/Fe_3O_4/MXene@AgNP fibers; and (d) representative EDX image of composite nanofibers.

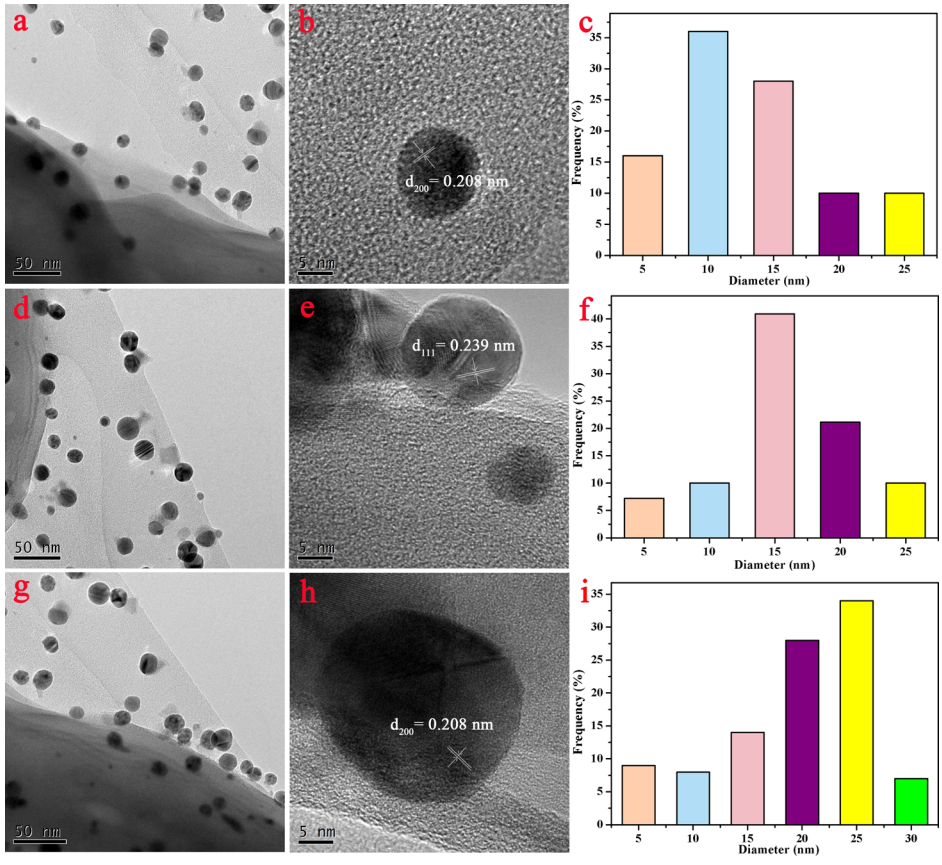

Figure 5. (a,d,g) TEM images of the PVA/PAA/Fe_3O_4/MXene composite nanofibers after loaded Ag NPs at 10, 20, and 60 min; (b,e,h) high-resolution TEM images, and (c,f,i) particle size distribution of Ag NPs at (a,d,g).

DOI: 10.1021/acsomega.8b03615
ACS Omega 2019, 4, 1897−1906

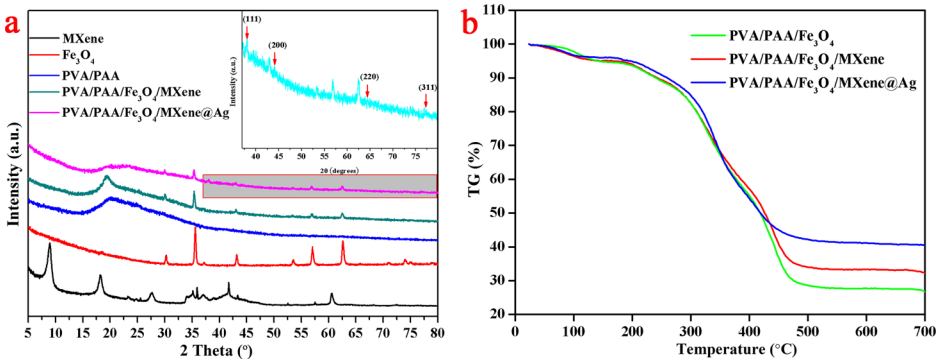

Figure 6. XRD patterns (a) and TG curves (b) of the prepared different composite nanofibers. The inset shows the illustration of the partial enlargement in the XRD curve of PVA/PAA/Fe_3O_4/MXene@AgNP composite.

AgNPs in the XRD pattern corresponding to the (111), (200), (220), and (311) planes, which further confirmed the loading of AgNPs successfully. As shown in Figure 6b, the thermal stability of different composite nanofibers was measured. The weight loss was observed at 150 °C, which indicated that the absorbed water was removed. Also, from 280 to 480 °C, the sharp weight loss could be because of the thermal decomposition of carbon chain. The weight values of the samples remained constant when the temperature reached 500 °C.[36,37] Furthermore, it indicated that the PVA/PAA/Fe_3O_4/MXene@AgNP composite nanofibers demonstrated better thermal stability. The heat loss of the PVA/PAA/Fe_3O_4 composite nanofibers was 72.55%, whereas the PVA/PAA/Fe_3O_4/MXene and PVA/PAA/Fe_3O_4/Mxene@AgNP composite nanofibers lost 66.94 and 58.8%, respectively. The difference in heat loss was mainly because of the addition of MXene nanosheets and the loading of AgNPs.

Magnetic properties of different samples were investigated at room temperature using magnetization hysteresis loops, as shown in Figure 7. The fully reversible field-dependent

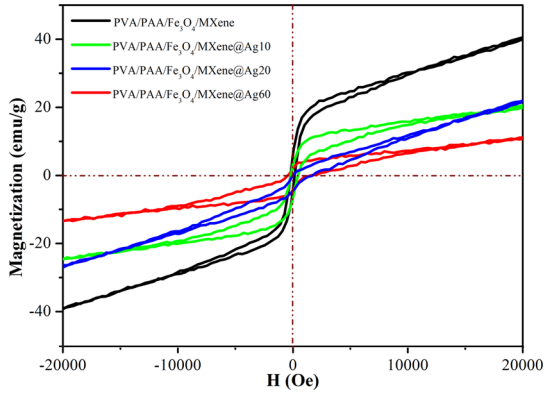

Figure 7. Magnetization hysteresis loops of PVA/PAA nanofibers and PVA/PAA/Fe_3O_4/MXene-loaded Ag NPs at 10, 20, and 60 min.

magnetization curve proved that all materials were superparamagnetic with no coercivity and remanence.[37] The PVA/PAA/Fe_3O_4/MXene composite nanofibers showed 39.9 emu/g saturation magnetization values at 20 kOe.[37−40] The saturation magnetization value was reduced to 10.9 emu/g after AgNPs were loaded for 60 min. The saturation magnetization decreased with the prolongation of AgNP loading.[37] The saturation magnetization of PVA/PAA/Fe_3O_4/Mxene@AgNPs was 22.3 and 19.33 emu/g at 10 and 20 min, respectively.

We used X-ray photoelectron spectroscopy (XPS) technique to study and investigate the elemental components and composition. The XPS patterns indicated the characteristic peaks of C 1s, O 1s, and Ag 3d, as shown in Figure 8a. The obvious peaks at 368 and 374 eV from AgNPs in samples were assigned to Ag $3d_{5/2}$ and Ag $3d_{3/2}$,[42] as shown in Figure 8b. This indicated that AgNPs existed in the form of a simple substance. Similarly, the peaks at 718.8 and 736.4 eV correspond to Fe $2p_{1/2}$ and Fe $2p_{3/2}$, respectively. In addition, we analyzed the oxygen and carbon elements and found that the peak positions at 284.5 eV and 285.7 represented C−C, C−OH, C−O, C═O, and O═C−O, respectively. The peak positions at 532.1 and 532.8 eV represented C−O bond and C═O bonds, respectively. Figure 8f showed an energy spectrum (EDS) of the composite nanofibers, showing that the composite fibers contained carbon, oxygen, iron, and silver elements. In summary, the above results indicated that the obtained AgNPs had been successfully anchored on composite nanofibers.

2.2. Catalytic Performances of Composite Fibers. The catalytic reaction of PVA/PAA/Fe_3O_4/Mxene@AgNP composite nanofibers on nitro compounds could reflect their catalytic properties. To investigate the catalytic activity of the composite nanofibers, fresh $NaBH_4$ aqueous solution (20 mL, 0.01 mol/L) was poured into 2-NA (2 mL, 5 mmol/L) or 4-NP (2 mL, 5 mmol/L), and then composite nanofibers were placed in a solution to measure their reducibility by UV−vis spectroscopy at room temperature.[43−46] Figure 9a showed that the UV−vis absorption peak of 4-NP changes from 317 to 402 nm after $NaBH_4$ was added, which was due to the formation of 4-nitrophenolate. The color of 4-NP and $NaBH_4$ mixture unchanged for 24 h without catalyst indicated that the reaction did not occur. After the addition of the composite nanofibers, the peak of 4-NP gradually decreased at 402 nm until it no longer changed, which means that 4-NP was completely reduced (Figure 9b). In the experiment, the concentration of $NaBH_4$ was 400 times than that of 4-NP, and the whole process of catalyzing 4-NP could be regarded as the pseudo-first-order reaction. A linear relationship between $\ln(C_t/C_0)$ and time (t) in the catalytic reaction was shown in Figure 9c, demonstrating that the catalytic reaction fitted pseudo-first-order reaction (C_t-concentration, C_0-initial concentration, and t-time). The reaction rate of the catalytic reaction was 0.168 min^{-1} (Figure 9c), suggesting that the PVA/PAA/Fe_3O_4/Mxene@AgNP20 composite nanofibers showed good catalytic activity for 4-NP.

DOI: 10.1021/acsomega.8b03615
ACS Omega 2019, 4, 1897−1906

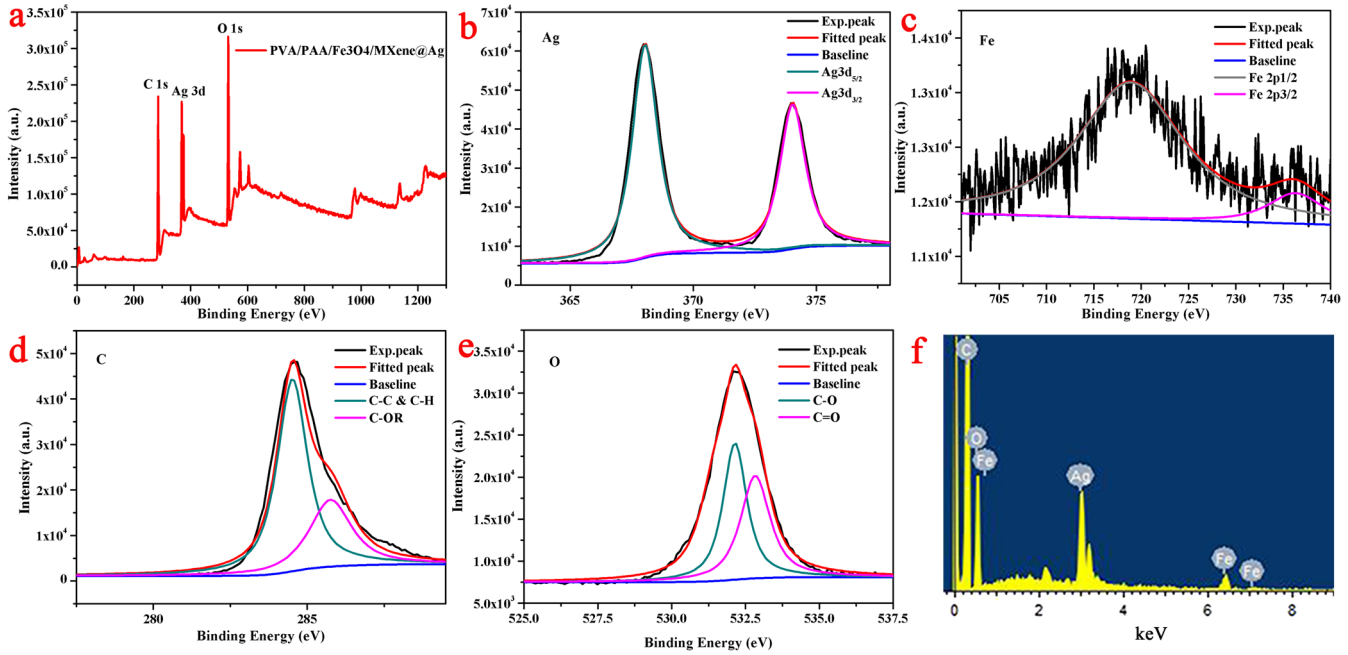

Figure 8. (a) XPS profiles of the PVA/PAA/Fe_3O_4/MXene@AgNP nanofibers. The XPS of elements: (b) Ag, (c) Fe, (d) C, and (e) O in the composite nanofibers. (f) Representative EDS image of the PVA/PAA/Fe_3O_4/MXene@AgNP nanofibers.

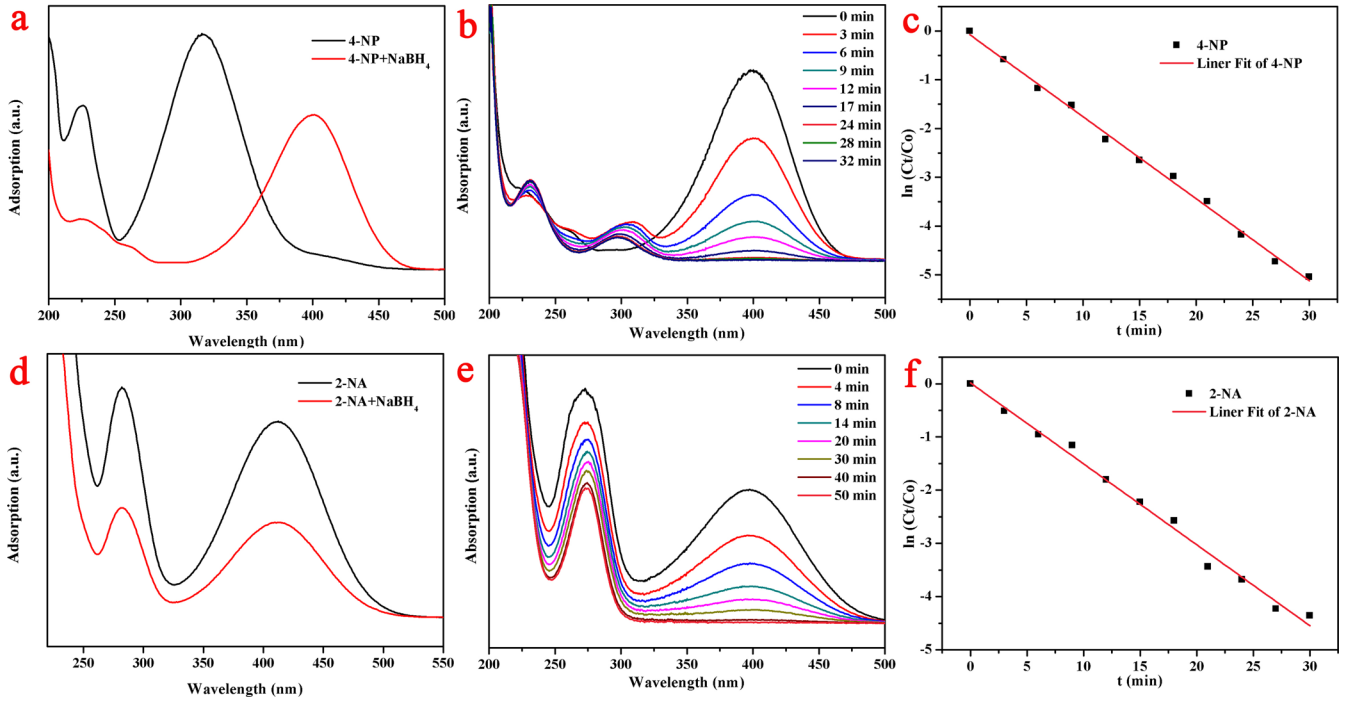

Figure 9. UV−vis spectra of (a) 4-NP and (d) 2-NA before and after adding $NaBH_4$ aqueous solution; (b,e) catalytic reduction of 4-NP or 2-NA with PVA/PAA/Fe_3O_4/MXene@AgNP20 composite nanofibers; and (c,f) relationship between $\ln(C_t/C_0)$ and the reaction time (t) of composite nanofiber catalyst.

To further evaluate the catalytic activity of the composite nanofibers, we conducted a 2-NA catalytic reaction experiment.[51] The color of 4-NA and $NaBH_4$ mixture remained unchanged for 24 h without the catalyst. The UV−vis absorption peak position of 2-NA was still at 415 nm after adding $NaBH_4$, as shown in Figure 9d. After adding an appropriate amount of composite fiber, the catalytic reaction was completed within 1 h, and the catalytic effect of the composite fiber was shown in (Figure 9e). Similarly, the catalytic reaction of the composite nanofibers to 2-NA could also be considered as a pseudo-first-order reaction (Figure 9f). The reaction rate of the catalytic reaction was 0.152 min^{-1}, which proved that the complex had a good catalytic activity for 2-NA. In addition, we also evaluated the catalytic performances of the other two samples (PVA/PAA/Fe_3O_4/Mxene@AgNP10 and PVA/PAA/Fe_3O_4/Mxene@AgNP60) for 4-NP and 2-NA, and the completed time of the catalytic reaction for 4-Np and 2-NA seemed larger than 90 min, which showed a similar

DOI: 10.1021/acsomega.8b03615
ACS Omega 2019, 4, 1897−1906

phenomenon in our previous MXene-AuNP system.[43] In addition, in the present study, the combination of MXene with PAA and PVA could improve the dispersion and surface area of MXene sheets, enhancing the active sites for reduction and loading of Ag NPs. Moreover, the addition of Fe_3O_4 enabled the composites to be easily recycled.

3. CONCLUSIONS

In conclusion, new AgNP-loaded PVA/PAA/Fe_3O_4/MXene composite nanofiber materials were prepared via electrospinning technology and self-reduction reaction of MXene flakes with $AgNO_3$. The MXene flakes, scaled from 200 to 400 nm, were successfully stripped on multilayer MXene by DMSO intercalation and subsequent sonication, and large-scale dispersion was achieved. The MXene nanosheets embedded in the fiber by electrospinning technology not only achieved high-dispersion targets but also retained its own physicochemical properties. By controlling the time of the self-reduction reaction, it seemed a facile approach to prepare AgNP-loaded fiber composites with different particle sizes and exhibited different catalytic properties for 2-NA and 4-NP. The PVA/PAA/Fe_3O_4/MXene@AgNP composite nanofibers exhibited excellent reactive activity for the catalytic reaction of certain nitro compounds (such as 2-NA and 4-NP), which was attributed to the special structural characteristics of the composite nanofibers and the good Ag-based catalytic activity. Moreover, the composite nanofiber materials could exhibit magnetic properties because of the addition of Fe_3O_4 NPs. The experimental results showed that the obtained PVA/PAA/Fe_3O_4/MXene@AgNP20 composite nanofibers displayed the best catalytic performance. Thus, the present work provided a new idea for the preparation of new MXene-based composite nanomaterials for wastewater treatment.

4. EXPERIMENTAL SECTION

4.1. Materials and Instruments. PVA (MW 57 000−66 000, 98−99% hydrolyzed), poly(acrylic acid) (PAA, MW ≈ 2000), 4-NP, and 2-NA were purchased from Aladdin Reagent (Shanghai, China). Fe_3O_4 and MXene ($Ti_3C_2T_x$) were synthesized in the laboratory according to previous studies.[52−54] $AgNO_3$ (98%) was obtained from Tianyi (Tianjin, China). DMSO (99%) and sodium borohydride ($NaBH_4$, 98%) were purchased from Kermel Chemicals (Tianjin, China) and Alfa Aesar (Beijing, China), respectively. All chemicals used in this experiment were without further purification. Ultrapure water was purified by the experimental Milli-Q Millipore filter system which was purchased from Millipore Corporation (USA).

SEM (Hitachi S4800, Ibaraki, Japan) and TEM (Hitachi HT7700, Ibaraki, Japan) were used to characterize sample morphology. The HRTEM images were obtained by a JEM-2010 electron microscope at 200 kV. A SMART LAB X-ray diffractometer (Rigaku, Japan) with a Bragg diffraction apparatus and a Cu Kα X-ray radiation source were utilized to get XRD patterns. Catalytic experiments were measured by UV-2550 spectrophotometer. XPS analysis was obtained by a Thermo Scientific ESCALAB 250Xi XPS (San Jose, CA, USA) with 200 W monochromatic Al Kα radiations. The magnetization was performed by MPMS-XL superconducting quantum interference device magnetometer (San Diego, CA, USA) at a temperature of 300 K. Thermogravimetry (TG) analysis was performed by a simultaneous thermal analyzer (NETZSCH STA 409 PC Luxx, Seligenstadt, Germany) under argon atmosphere.

4.2. Sample Preparation. Multilayer MXene ($Ti_3C_2T_x$) was obtained by etching the Al element from MAX (Ti_3AlC_2) via HF acid. MXene flake colloidal suspension was prepared by powder separation and water bath sonication (Shenhuatai SUS304 Ultrasonic bath, 110 W and 40 kHz). In short, 36 mg of MXene powder was mixed with 2 mL of DMSO and then magnetically stirred at 18 °C for 18 h to ensure that DMSO was intercalated in the multilayer structure of MXene. The intercalated MXene mixture would be centrifuged at 3500 rpm for 15 min to obtain a solid powder after removal of the supernatant. Then, 9 mL of ultrapure water was added to the DMSO-intercalated MXene residue at 10 °C. After a weak sonication with 110 W and 40 kHz frequency, the few MXene with intercalated DMSO were dispersed in ultrapure water. Fully delaminated Ti_3C_2 flake colloidal solutions were obtained. The residue was removed by centrifugation at 3500 rpm for 1 h to obtain a dark green MXene foil colloidal solution. The sizes of the nanosheets were mostly 200−500 nm, and the colloidal solution was relatively stable.

PVA (0.5 g) was added to 4.5 g of the colloidal solution of MXene flakes to form 10 wt % solutions and then stirred at 80 °C for 12 h. Fe_3O_4 (50 mg) solid was added to the above PVA solution and stirred for 1 h at 25 °C. PAA (0.6 g) was added to 1.4 g of MXene flake colloid solution to form 30 wt % solution and then stirred at 25 °C for 1 h. We mixed all of the solutions together and stirred at 25 °C until uniform, which was the spinning precursor solution for next steps. During the electrospinning process, a 10 mL syringe load of PVA/PAA/Fe_3O_4/MXene precursor solution was connected to a stainless steel needle through a thin tube. We choose the optimal parameter conditions: 15 kV (needle tip voltage)-20 cm (working distance)-0.5 mL/h (feed rate of solutions). Then, spinning was carried out at 25 °C and 40% humidity. The obtained electrospun nanofibers were deposited on the surface of the aluminum foil and then dried in vacuum at 25 °C for 24 h. After that, heat-induced cross-linking reaction of the obtained electrospun nanofibers occurred when heated at 120 °C for 5 h.[31] After thermal treatment and heat-induced cross-linking reaction, PVA/PAA/Fe_3O_4/MXene membranes were insoluble in water because of the esterification reaction between some of the partial hydroxyl groups and carboxylic acid groups. Next, the spun fiber membrane was immersed into 2.5 mg/mL $AgNO_3$ solution and gently stirred at 25 °C for Ag NP reduction growth. The PVA/PAA/Fe_3O_4/MXene@AgNP composite nanofibers were obtained with different immersion times (10, 20, and 60 min, respectively). The composite nanofibers were then taken out of $AgNO_3$ aqueous solution, washed with ultrapure water three times to remove non-adhered or free $AgNO_3$ NPs, and then dried at 30 °C for 24 h in vacuum.

4.3. Catalytic Performance Test. The catalytic performance of PVA/PAA/Fe_3O_4/MXene@AgNP electrospun nanofibers was determined by catalytic reduction of the solutions of 4-NP and 2-NA.[55−60] The reducing agent selected in the catalytic reduction reaction was $NaBH_4$, and the whole reaction process was carried out under ultraviolet spectrum detection at 25 °C.[47] 4-NP aqueous solution (10 mL, 0.005 M) was prepared, and fresh aqueous $NaBH_4$ solution (20 mL, 0.1 M) was added, and then PVA/PAA/Fe_3O_4/MXene@AgNP (40 mg) was added to the mixed solution for 60 min (named as PVA/PAA/Fe_3O_4/MXene @ AgNP60). The

DOI: 10.1021/acsomega.8b03615
ACS Omega 2019, 4, 1897−1906

absorbance of the mixed solution was monitored by UV−vis spectroscopy every 3 min until the absorbance of the solution was minimized and remained unchanged. At the same time, we evaluated the catalytic ability of nanofibers by catalyzing 2-NA (10 mL, 0.005 M) aqueous solution again. After the catalysis was completed, the nanofiber sample can be taken out by an external magnetic field.[61−64]

AUTHOR INFORMATION

Corresponding Authors

*E-mail: tfjiao@ysu.edu.cn (T.J.).
*E-mail: pengqiuming@ysu.edu.cn (Q.P.).

ORCID

Tifeng Jiao: 0000-0003-1238-0277
Qiuming Peng: 0000-0002-3053-7066

Author Contributions

§X.H. and R.W. contributed equally to this work.

Notes

The authors declare no competing financial interest.

ACKNOWLEDGMENTS

This work was financially supported by the National Natural Science Foundation of China (nos. 21872119 and 21473153), support program for the Top Young Talents of Hebei Province, China Postdoctoral Science Foundation (no. 2015M580214), Research Program of the College Science & Technology of Hebei Province (no. ZD2018091), and Scientific and Technological Research and Development Program of Qinhuangdao City (no. 201701B004).

REFERENCES

(1) Lukatskaya, M. R.; Mashtalir, O.; Ren, C. E.; Dall'Agnese, Y.; Rozier, P.; Taberna, P. L.; Naguib, M.; Simon, P.; Barsoum, M. W.; Gogotsi, Y. Cation intercalation and high volumetric capacitance of two-dimensional titanium carbide. *Science* **2013**, *341*, 1502−1505.

(2) Jian, M.; Wang, C.; Wang, Q.; Wang, H.; Xia, K.; Yin, Z.; Zhang, M.; Liang, X.; Zhang, Y. Advanced carbon materials for flexible and wearable sensors. *Sci. China Mater.* **2017**, *60*, 1206−1062.

(3) Li, Z.; Wang, L.; Sun, D.; Zhang, Y.; Liu, B.; Hu, Q.; Zhou, A. Synthesis and thermal stability of two-dimensional carbide MXene Ti_3C_2. *Mater. Sci. Eng., B* **2015**, *191*, 33−40.

(4) Naguib, M.; Mochalin, V. N.; Barsoum, M. W.; Gogotsi, Y. 25th anniversary article: MXenes: a new family of two-dimensional materials. *Adv. Mater.* **2013**, *26*, 992−1005.

(5) Li, J.; Du, Y.; Huo, C.; Wang, S.; Cui, C. Thermal stability of two-dimensional Ti_2C nanosheets. *Ceram. Int.* **2015**, *41*, 2631−2635.

(6) Miranda, A.; Halim, J.; Barsoum, M. W.; Lorke, A. Electronic properties of freestanding $Ti_3C_2T_x$ MXene monolayers. *Appl. Phys. Lett.* **2016**, *108*, 033102.

(7) Boota, M.; Anasori, B.; Voigt, C.; Zhao, M.-Q.; Barsoum, M. W.; Gogotsi, Y. Pseudocapacitive electrodes produced by oxidant-free polymerization of pyrrole between the layers of 2D titanium carbide (MXene). *Adv. Mater.* **2015**, *28*, 1517−1522.

(8) Zou, G.; Zhang, Z.; Guo, J.; Liu, B.; Zhang, Q.; Fernandez, C.; Peng, Q. Synthesis of MXene/Ag composites for extraordinary long cycle lifetime lithium storage at high rates. *ACS Appl. Mater. Interfaces* **2016**, *8*, 22280−22286.

(9) Wang, H.; Zhang, J.; Wu, Y.; Huang, H.; Li, G.; Zhang, X.; Wang, Z. Surface modified MXene Ti_3C_2, multilayers by aryl diazonium salts leading to large-scale delamination. *Appl. Surf. Sci.* **2016**, *384*, 287−293.

(10) Lin, S.-Y.; Zhang, X. Two-dimensional titanium carbide electrode with large mass loading for supercapacitor. *J. Power Sources* **2015**, *294*, 354−359.

(11) Karlsson, L. H.; Birch, J.; Halim, J.; Barsoum, M. W.; Persson, P. O. Å. Atomically resolved structural and chemical investigation of single MXene sheets. *Nano Lett.* **2015**, *15*, 4955−4960.

(12) Vaughn, A.; Ball, J.; Heil, T.; Morgan, D. J.; Lampronti, G. I.; Maršalkaitė, G.; Raston, C. L.; Power, N. P.; Kellici, S. Selective calixarene-directed synthesis of MXene plates, crumpled sheets, spheres, and scrolls. *Chem.—Eur. J.* **2017**, *23*, 8128−8133.

(13) Syamsai, R.; Kollu, P.; Kwan Jeong, S.; Nirmala Grace, A. Synthesis and properties of 2D-Titanium carbide MXene sheets towards electrochemical energy storage applications. *Ceram. Int.* **2017**, *43*, 13119−13126.

(14) Zhao, M.-Q.; Ren, C. E.; Ling, Z.; Lukatskaya, M. R.; Zhang, C.; Van Aken, K. L.; Barsoum, M. W.; Gogotsi, Y. Flexible MXene/carbon nanotube composite paper with high volumetric capacitance. *Adv. Mater.* **2014**, *27*, 339−345.

(15) Er, D.; Li, J.; Naguib, M.; Gogotsi, Y.B.; Shenoy, V. B. Ti_3C_2 MXene as a high capacity electrode material for metal (Li, Na, K, Ca) ion batteries. *ACS Appl. Mater. Interfaces* **2014**, *6*, 11173−11179.

(16) Ghidiu, M.; Naguib, M.; Shi, C.; Mashtalir, O.; Pan, L. M.; Zhang, B.; Yang, J.; Gogotsi, Y.; Billinge, S. J. L.; Barsoum, M. W. Synthesis and characterization of two-dimensional Nb_4C_3 (MXene). *Chem. Commun.* **2014**, *50*, 9517−9520.

(17) Xie, Y.; Dall'Agnese, Y.; Naguib, M.; Gogotsi, Y.; Barsoum, M. W.; Zhuang, H. L.; Kent, P. R. C. Prediction and characterization of MXene nanosheet anodes for non-lithium-ion batteries. *ACS Nano* **2014**, *8*, 9606−9615.

(18) Liang, X.; Garsuch, A.; Nazar, L. F. Sulfur cathodes based on conductive MXene nanosheets for high-performance lithium-sulfur batteries. *Angew. Chem., Int. Ed.* **2015**, *54*, 3907−3911.

(19) Khazaei, M.; Arai, M.; Sasaki, T.; Estili, M.; Sakka, Y. Two-dimensional molybdenum carbides: potential thermoelectric materials of the MXene family. *Phys. Chem. Chem. Phys.* **2014**, *16*, 7841−7849.

(20) Ma, Z.; Hu, Z.; Zhao, X.; Tang, Q.; Wu, D.; Zhou, Z.; Zhang, L. Tunable band structures of heterostructured bilayers with transition-metal dichalcogenide and MXene monolayer. *J. Phys. Chem. C* **2014**, *118*, 5593−5599.

(21) Aïssa, B.; Ali, A.; Mahmoud, K. A.; Haddad, T.; Nedil, M. Transport properties of a highly conductive 2D Ti_3C_2Tx MXene/graphene composite. *Appl. Phys. Lett.* **2016**, *109*, 043109.

(22) Hope, M. A.; Forse, A. C.; Griffith, K. J.; Lukatskaya, M. R.; Ghidiu, M.; Gogotsi, Y.; Grey, C. P. NMR reveals the surface functionalisation of Ti_3C_2 MXene. *Phys. Chem. Chem. Phys.* **2016**, *18*, 5099−5102.

(23) Gao, Y.; Wang, L.; Li, Z.; Zhou, A.; Hu, Q.; Cao, X. Preparation of MXene-Cu_2O nanocomposite and effect on thermal decomposition of ammonium perchlorate. *Solid State Sci.* **2014**, *35*, 62−65.

(24) Shi, C.; Beidaghi, M.; Naguib, M.; Mashtalir, O.; Gogotsi, Y.; Billinge, S. J. L. Structure of nanocrystalline Ti_3C_2 MXene using atomic pair distribution function. *Phys. Rev. Lett.* **2014**, *112*, 125501.

(25) Ren, C. E.; Hatzell, K. B.; Alhabeb, M.; Ling, Z.; Mahmoud, K. A.; Gogotsi, Y. Charge- and size-selective ion sieving through $Ti_3C_2T_x$ MXene membranes. *J. Phys. Chem. Lett.* **2015**, *6*, 4026−4031.

(26) Ling, Z.; Ren, C. E.; Zhao, M.-Q.; Yang, J.; Giammarco, J. M.; Qiu, J.; Barsoum, M. W.; Gogotsi, Y. Flexible and conductive MXene films and nanocomposites with high capacitance. *Proc. Natl. Acad. Sci. U.S.A.* **2014**, *111*, 16676−16681.

(27) Wang, F.; Yang, C.; Duan, C.; Xiao, D.; Tang, Y.; Zhu, J. An organ-like titanium carbide material (MXene) with multilayer structure encapsulating hemoglobin for a mediator-free biosensor. *J. Electrochem. Soc.* **2015**, *162*, B16−B21.

(28) Shein, I. R.; Ivanovskii, A. L. Graphene-like titanium carbides and nitrides Ti_{n+1} C_n, Ti_{n+1} N_n, (n =1,2 and 3) from de-intercalated MAX phases: First-principles probing of their structural, electronic properties and relative stability. *Comput. Mater. Sci.* **2012**, *65*, 104−114.

(29) Cygan, R. T.; Liang, J.-J.; Kalinichev, A. G. Molecular models of hydroxide, oxyhydroxide, and clay phases and the development of a general force field. *J. Phys. Chem. B* **2004**, *108*, 1255−1266.

DOI: 10.1021/acsomega.8b03615
ACS Omega 2019, 4, 1897−1906

(30) Eklund, P.; Beckers, M.; Jansson, U.; Högberg, H.; Hultman, L. The $M_{n+1}AX_n$ phases: Materials science and thin-film processing. *Thin Solid Films* **2010**, *518*, 1851−1878.
(31) Liu, K.; Yuan, C.; Zou, Q.; Xie, Z.; Yan, X. Self-Assembled Zinc/Cystine-Based Chloroplast Mimics Capable of Photoenzymatic Reactions for Sustainable Fuel Synthesis. *Angew. Chem., Int. Ed.* **2017**, *56*, 7876−7880.
(32) Liu, K.; Xing, R.; Li, Y.; Zou, Q.; Möhwald, H.; Yan, X. Mimicking Primitive Photobacteria: Sustainable Hydrogen Evolution Based on Peptide-Porphyrin Co-Assemblies with a Self-Mineralized Reaction Center. *Angew. Chem., Int. Ed.* **2016**, *55*, 12503−12507.
(33) Liu, K.; Xing, R.; Chen, C.; Shen, G.; Yan, L.; Zou, Q.; Ma, G.; Möhwald, H.; Yan, X. Peptide-induced hierarchical long-range order and photocatalytic activity of porphyrin assemblies. *Angew. Chem., Int. Ed.* **2015**, *54*, 500−505.
(34) Abay, A. K.; Kuo, D.-H.; Chen, X.; Saragih, A. D. A new V-doped $Bi_2(O,S)_3$ oxysulfide catalyst for highly efficient catalytic reduction of 2-nitroaniline and organic dyes. *Chemosphere* **2017**, *189*, 21−31.
(35) Thirumalraj, B.; Rajkumar, C.; Chen, S.-M.; Lin, K.-Y. Determination of 4-nitrophenol in water by use of a screen-printed carbon electrode modified with chitosan-crafted ZnO nanoneedles. *J. Colloid Interface Sci.* **2017**, *499*, 83−92.
(36) Hou, C.; Jiao, T.; Xing, R.; Chen, Y.; Zhou, J.; Zhang, L. Preparation of TiO_2, nanoparticles modified electrospun nanocomposite membranes toward efficient dye degradation for wastewater treatment. *J. Taiwan Inst. Chem. Eng.* **2017**, *78*, 118−126.
(37) Guo, R.; Jiao, T.; Xing, R.; Chen, Y.; Guo, W.; Zhou, J.; Zhang, L.; Peng, Q. Hierarchical AuNPs-loaded Fe_3O_4/polymers nanocomposites constructed by electrospinning with enhanced and magnetically recyclable catalytic capacities. *Nanomaterials* **2017**, *7*, 317.
(38) Guo, R.; Jiao, T.; Li, R.; Chen, Y.; Guo, W.; Zhang, L.; Zhou, J.; Zhang, Q.; Peng, Q. Sandwiched Fe_3O_4/carboxylate graphene oxide nanostructures constructed by layer-by-layer assembly for highly efficient and magnetically recyclable dye removal. *ACS Sustainable Chem. Eng.* **2017**, *6*, 1279−1288.
(39) Li, X.; Lou, L.; Song, W.; Huang, G.; Hou, F.; Zhang, Q.; Zhang, H.-T.; Xiao, J.; Wen, B.; Zhang, X. Novel bimorphological anisotropic bulk nanocomposite materials with high energy products. *Adv. Mater.* **2017**, *29*, 1606430.
(40) Li, X.; Lou, L.; Song, W.; Zhang, Q.; Huang, G.; Hua, Y.; Zhang, H.-T.; Xiao, J.; Wen, B.; Zhang, X. Controllably manipulating three-dimensional hybrid nanostructures for bulk nanocomposites with large energy products. *Nano Lett.* **2017**, *17*, 2985−2993.
(41) Satheeshkumar, E.; Makaryan, T.; Melikyan, A.; Minassian, H.; Gogotsi, Y.; Yoshimura, M. One-step solution processing of Ag, Au and Pd@MXene hybrids for SERS. *Sci. Rep.* **2016**, *6*, 32049.
(42) Zou, G.; Zhang, Z.; Guo, J.; Liu, B.; Zhang, Q.; Fernandez, C.; Peng, Q. Synthesis of MXene/Ag composites for extraordinary long cycle lifetime lithium storage at high rates. *ACS Appl. Mater. Interfaces* **2016**, *8*, 22280−22286.
(43) Li, K.; Jiao, T.; Xing, R.; Zou, G.; Zhou, J.; Zhang, L.; Peng, Q. Fabrication of tunable hierarchical MXene@AuNPs nanocomposites constructed by self-reduction reactions with enhanced catalytic performances. *Sci. China Mater.* **2018**, *61*, 728−736.
(44) Li, K.; Jiao, T.; Xing, R.; Zou, G.; Zhao, Q.; Zhou, J.; Zhang, L.; Peng, Q. Fabrication of hierarchical MXene-based AuNPs-containing core-shell nanocomposites for high efficient catalysts. *Green Energy Environ.* **2018**, *3*, 147−155.
(45) Guo, W.; Jiao, J.; Tian, K.; Tang, Y.; Jia, Y.; Li, R.; Xu, Z.; Wang, H. Controllable synthesis of core−satellite Fe_3O_4@polypyrrole/Pd nanoarchitectures with aggregation-free Pd nanocrystals confined into polypyrrole satellites as magnetically recoverable and highly efficient heterogeneous catalysts. *RSC Adv.* **2015**, *5*, 102210−102218.
(46) Zhao, X.; Jiao, T.; Ma, X.; Huang, H.; Hu, J.; Qu, Y.; Zhou, J.; Zhang, L.; Peng, Q. Facile fabrication of hierarchical diamond-based AuNPs-modified nanocomposites via layer-by-layer assembly with enhanced catalytic capacities. *J. Taiwan Inst. Chem. Eng.* **2017**, *80*, 614−623.
(47) Hervés, P.; Pérez-Lorenzo, M.; Liz-Marzán, L. M.; Dzubiella, J.; Lu, Y.; Ballauff, M. Catalysis by metallic nanoparticles in aqueous solution: model reactions. *Chem. Soc. Rev.* **2012**, *41*, 5577−5587.
(48) Xing, R.; Wang, W.; Jiao, T.; Ma, K.; Zhang, Q.; Hong, W.; Qiu, H.; Zhou, J.; Zhang, L.; Peng, Q. Bioinspired polydopamine sheathed nanofibers containing carboxylate graphene oxide nanosheet for high-efficient dyes scavenger. *ACS Sustainable Chem. Eng.* **2017**, *5*, 4948−4956.
(49) Naguib, M.; Mashtalir, O.; Carle, J.; Presser, V.; Lu, J.; Hultman, L.; Gogotsi, Y.; Barsoum, M. W. Two-dimensional transition metal carbides. *ACS Nano* **2012**, *6*, 1322−1331.
(50) Mashtalir, O.; Naguib, M.; Mochalin, V. N.; Dall'Agnese, Y.; Heon, M.; Barsoum1, M. W.; Gogotsi, Y. Intercalation and delamination of layered carbides and carbonitrides. *Nat. Commun.* **2013**, *4*, 1716.
(51) Tan, L.; Chen, D.; Liu, H.; Tang, F. A silica nanorattle with a mesoporous shell: an ideal nanoreactor for the preparation of tunable gold cores. *Adv. Mater.* **2010**, *22*, 4885−4889.
(52) Jiao, J.; Wang, H.; Guo, W.; Li, R.; Tian, K.; Xu, Z.; Jia, Y.; Wu, Y.; Cao, L. In situ confined growth based on a self-templating reduction strategy of highly dispersed Ni nanoparticles in hierarchical yolk-shell Fe@SiO_2 structures as efficient catalysts. *Chem.—Asian J.* **2016**, *11*, 3534−3540.
(53) Zou, G.; Liu, B.; Guo, J.; Fernandez, C.; Peng, Q. Synthesis of nanoflower-shaped MXene derivative with unexpected catalytic activity for dehydrogenation of sodium alanates. *ACS Appl. Mater. Interfaces* **2017**, *9*, 7611−7618.
(54) Zhang, Q.; Teng, J.; Zou, G.; Peng, Q.; Du, Q.; Jiao, T.; Xiang, J. Efficient phosphate sequestration for water purification by unique sandwich-like MXene/magnetic iron oxide nanocomposites. *Nanoscale* **2016**, *8*, 7085−7093.
(55) Wang, C.; Sun, S.; Zhang, L.; Yin, J.; Jiao, T.; Zhang, L.; Xu, Y.; Zhou, J.; Peng, Q. Facile preparation and catalytic performance characterization of AuNPs-loaded hierarchical electrospun composite fibers by solvent vapor annealing treatment. *Colloids Surf., A* **2019**, *561*, 283−291.
(56) Sun, S.; Wang, C.; Han, S.; Jiao, T.; Wang, R.; Yin, J.; Li, Q.; Wang, Y.; Geng, L.; Yu, X.; Peng, Q. Interfacial nanostructures and acidichromism behaviors in self-assembled terpyridine derivatives Langmuir-Blodgett films. *Colloids Surf., A* **2019**, *564*, 1−9.
(57) Huang, X.; Jiao, T.; Liu, Q.; Zhang, L.; Zhou, J.; Li, B.; Peng, Q. Hierarchical electrospun nanofibers treated by solvent vapor annealing as air filtration mat for high-efficiency PM2.5 capture. *Sci. China Mater.* **2019**, *62*, 423−436.
(58) Xu, Y.; Ren, B.; Wang, R.; Zhang, L.; Jiao, T.; Liu, Z. Facile preparation of rod-like MnO nanomixtures via hydrothermal approach and highly efficient removal of methylene blue for wastewater Treatment. *Nanomaterials* **2019**, *9*, 10.
(59) Zhan, F.; Wang, R.; Yin, J.; Han, Z.; Zhang, L.; Jiao, T.; Zhou, J.; Zhang, L.; Peng, Q. Facile solvothermal preparation of Fe_3O_4−Ag nanocomposite with excellent catalytic performance. *RSC Adv.* **2019**, *9*, 878−883.
(60) Zhou, J.; Gao, F.; Jiao, T.; Xing, R.; Zhang, L.; Zhang, Q.; Peng, Q. Selective Cu(II) ion removal from wastewater via surface charged self-assembled polystyrene-Schiff base nanocomposites. *Colloids Surf., A* **2018**, *545*, 60−67.
(61) Gu, J.; Yin, B.; Fu, S.; Feng, M.; Zhang, Z.; Dong, H.; Gao, F.; Zhao, Y. S. Surface tension driven aggregation of organic nanowires via lab in a droplet. *Nanoscale* **2018**, *10*, 11006−11012.
(62) Gu, J.; Yin, B.; Feng, M.; Zhang, G.; Zhang, Z.; Zhong, J.; Zhang, C.; Wen, B.; Zhao, Y. S. Epitaxial growth of dual-color-emitting organic heterostructures via binary solvent synergism driven sequential crystallization. *Nanoscale* **2019**, 11.
(63) Luo, X.; Ma, K.; Jiao, T.; Xing, R.; Zhang, L.; Zhou, J.; Li, B. Graphene oxide-polymer composite Langmuir films constructed by interfacial thiol-ene photopolymerization. *Nanoscale Res. Lett.* **2017**, *12*, 99.

DOI: 10.1021/acsomega.8b03615
ACS Omega 2019, 4, 1897−1906

(64) Chen, K.; Li, J.; Zhang, L.; Xing, R.; Jiao, T.; Gao, F.; Peng, Q. Facile synthesis of self-assembled carbon nanotubes/dye composite films for sensitive electrochemical determination of Cd(II) ions. *Nanotechnology* **2018**, *29*, 445603.

DOI: 10.1021/acsomega.8b03615
ACS Omega 2019, 4, 1897−1906